

Unsupervised Discovery of Clinical Disease Signatures Using Probabilistic Independence

Thomas A. Lasko¹ John M. Still¹ Thomas Z. Li² Marco Barbero Mota¹
 William W. Stead¹ Eric V. Strobl¹ Bennett A. Landman²
 Fabien Maldonado¹

¹Vanderbilt University Medical Center, Nashville, TN

²Vanderbilt University, Nashville, TN

Abstract

Insufficiently precise diagnosis of clinical disease is likely responsible for many treatment failures, even for common conditions and treatments. With a large enough dataset, it may be possible to use unsupervised machine learning to define clinical disease patterns more precisely. We present an approach to learning these patterns by using probabilistic independence to disentangle the imprint on the medical record of causal latent sources of disease. We inferred a broad set of 2000 clinical signatures of latent sources from 9195 variables in 269,099 Electronic Health Records. The learned signatures produced better discrimination than the original variables in a lung cancer prediction task unknown to the inference algorithm, predicting 3-year malignancy in patients with no history of cancer before a solitary lung nodule was discovered. More importantly, the signatures' greater explanatory power identified pre-nodule signatures of apparently undiagnosed cancer in many of those patients.

1 Introduction

A meaningful fraction of treatment failures for common medical conditions may be due to insufficiently precise diagnoses [1–8]. Existing diagnostic and treatment protocols have been developed using expert clinical judgement, biochemical and molecular research, and large-scale clinical trials. They have served us well for the past century, but higher-precision treatment decisions will inevitably require higher-resolution diagnostic clinical pictures. We view *phenotype discovery* as the work of learning those pictures from Electronic Health Records (EHRs) using data-driven computational methods [9].

Our simplified mental model treats a patient's medical record as the result of a stochastic process that generates elements to appear in the record. The process is controlled by a set of

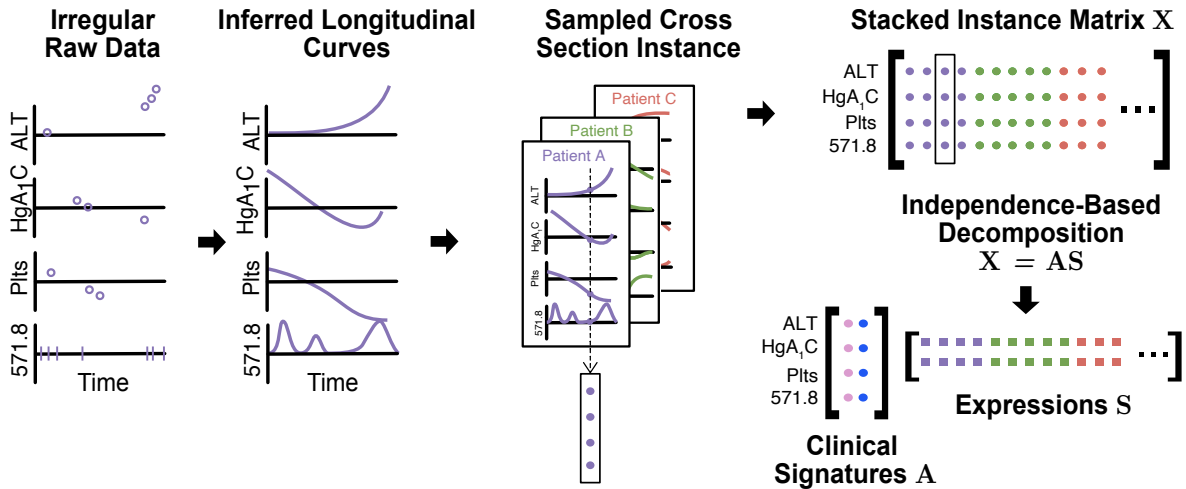


Figure 1: The pipeline for learning clinical signatures and their patient-level expressions from noisy, asynchronous, and irregular EHR data. The first three steps transform the data into a dense, regular matrix \mathbf{X} for machine learning. The final step infers the clinical signatures \mathbf{A} and the expression levels \mathbf{S} of latent disease sources using probabilistic independence.

probability distributions that vary over time and between patients. When a patient develops a new medical condition, that condition causes a set of changes to those distributions. We call that set of changes the *clinical signature* of the condition. We consider the condition itself to be an unobserved or latent source for those changes, and multiple latent sources may be active in a given patient at a given time. The sources do not act directly on the record, but they shape the probability distributions that govern the data generating process.

For example, a patient who develops type 2 diabetes will experience an increased probability per unit time that a `type 2 diabetes` billing code will appear in her record, and a smaller but nonzero increase in the probability that an (incorrect) `type 1 diabetes` code will appear. (For clarity, we use an `alternate font` for names of observed variables.) The condition may also cause, among other things, changes to the distribution of `hemoglobin A1C` values, to the distribution of `blood glucose` values and the frequency of measuring them, and to the probability that `metformin` will appear as a medication. These probabilities evolve as the condition progresses, with late-stage disease producing greater changes in blood chemistry and in code density for end-organ failure. In early stage disease, elements may appear due to the mere suspicion of a condition, representing attempts to diagnose or rule out disease. Representing EHR elements as probabilistic events generated by a stochastic process allows for these investigative actions, typical documentation errors, measurement noise, and visit timing to act as evidence for or against the presence of a particular disease.

Representing the relevant probabilities as continuous longitudinal curves transforms the sparse and irregular EHR data into a form more amenable to machine learning [9, 10] (Figure

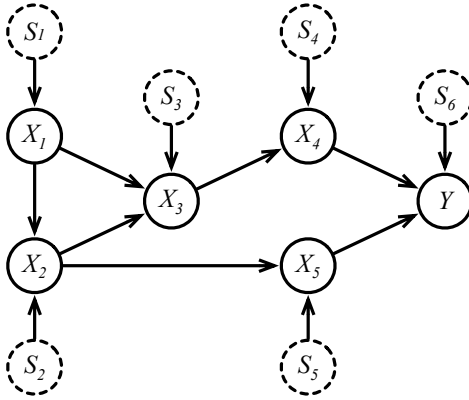


Figure 2: Example causal graph showing observed variables X_i , label Y , and unobserved (latent) sources S_i .

1). For example, the discrete events of diagnosis and procedure codes appearing in the record can be transformed into a continuous intensity curve of a non-homogeneous Gamma process [11]; irregularly measured laboratory values can be transformed into a continuous Gaussian process that represents a distribution over all value trajectories that could have produced the observed data [9, 12]; the discrete decisions to order the test itself can also be represented as a Gamma process [12]; and medication records can be transformed into continuous curves of total daily dose, or in cases of incomplete data, curves representing the probability that the patient took the given medication on a given day. Once the curves are computed for a given record, a cross section of all of their values at a given time may be extracted to estimate a patient’s clinical state at that moment, and a matrix of stacked cross sections from all records provides a dense, regular dataset for further analysis.

The central difficulty in learning clinical signatures comes from the fact that patients experience multiple simultaneous conditions, so the record is a confluence of overlapping observations, and the inference task is to disentangle the active signatures from those observations.

This paper provides an introduction to and real-world evaluation of an approach to using probabilistic independence to perform the disentangling. It expands on a preliminary report [10], analyses of the underlying theory [13–15], and some early applications [16, 17].

There are both empirical and theoretical reasons why we use this approach. Empirically, we found early in our work that clinical signatures identified using independence appear more coherent and clinically recognizable than those found using other disentangling methods, such as Singular Value Decomposition [18–20], Latent Dirichlet Allocation (LDA) [21], or various types of deep autoencoders [22–27]. On an analogous task in the genomic domain, objectively comparing 42 different methods of inferring groups of genes that are functionally related and co-regulated, investigators found that independence-based methods outperformed all

others [28]. A different group found that transcriptome structure inferred using Independent Component Analysis (ICA) was conserved across five datasets, despite those datasets coming from different research groups using different technologies [29].

Most importantly, under certain reasonable assumptions of causal inference, clinical signatures inferred using probabilistic independence have been shown theoretically to reflect root causes of disease [13–15], at least as far as those causes can be identified using the variables in the dataset. For example, suppose we have the causal graph formed by the observed variables X_i and label Y in Figure 2. The value of each observed X_i is a function of its parents, including an unobserved latent source S_i . We can think of the graph as existing in a steady state until a latent source changes its value, which then affects downstream variables. Those effects follow a specific pattern A_i (which we’ve been calling the clinical signature of the source), that depends on the presence and strength of causal relationships in the relevant parts of the network. For example, if source S_1 changes, it may affect any of the X_i and Y , but if S_4 changes, it can only affect X_4 and Y .

The key property of the S_i values (which we call source *expressions*) is that they are all mutually independent (as in Figure 2), and this property is exploited to make the inference. Methods such as ICA [30, 31] and Linear Non-Gaussian Acyclic Models (LiNGAM) [32, 33] can be used to recover the causal graph, the source signatures A_i , and the source expressions S_i from a matrix \mathbf{X} of many instances of observed values. This is done with unsupervised learning over \mathbf{X} alone, without the guidance of any label Y . Under these methods (including our use here), the relationship between \mathbf{X} and \mathbf{S} is assumed linear and additive, so that $\mathbf{X} = \mathbf{A}\mathbf{S}$, but inference of nonlinear relationships is a topic of current research [14, 34, 35]. The graph and the signatures remain fixed, with the expressions \mathbf{S} allowed to vary between patients and over time, inferred from changes in the observed data \mathbf{X} .

We can build a supervised model to predict a target Y (such as a binary disease label) from the expressions \mathbf{S} , and use Shapley values [36, 37] to identify the contribution of each source to the prediction for each patient, accounting for all possible combinations of predictors. Under this construction, the S_i that produce meaningfully non-zero contributions should, in theory, represent root causes of Y for that patient [13]. This is not the case when we use the observed \mathbf{X} as the predictive inputs; we can find strong *predictive associations* between \mathbf{X} and Y , but in general we cannot make causal claims using \mathbf{X} without careful conditioning or other specific analyses.

Phenotype discovery differs from the more common task of *computational phenotyping*, in which expert knowledge is used to define computable rule sets by which known diseases can be recognized in a given patient’s record [38–40]. The difference is that in phenotype discovery, we want to *let the data speak*, to tell *us* what the signatures of all the latent sources are, allowing us to discover emerging diseases, previously unrecognized conditions, and more precise definitions.

Prior Work This research derives from our early work inferring clinical signatures from EHR data [9, 10, 12, 41]. Much work by others since then has focused on the broader task of representation learning, in which features are sought purely for their predictive power, without attempting to learn clinical patterns reflecting different causes [42–48].

Some prior work attempts to infer meaningful clinical patterns using other approaches. Graph Convolutional Transformers have been proposed to learn functional relationships among diagnosis, treatment, and lab test codes while simultaneously using the inferred graph for clinical prediction tasks [49]. LDA uses a defined probabilistic graphical model to guide the decomposition of a data matrix into signature-like ‘topics’ [21]. Early work using LDA for phenotype discovery used separately parameterized distributions for each mode (text, lab orders, billing codes, medications), which implicitly avoided mode imbalance problems and produced 250 signatures, about 60% of which were judged by clinicians to be conceptually coherent [50]. Later work modified LDA inference to allow for missing data, and constructed the model in two layers to avoid the imbalance problem, producing 75 learned signatures [51]. Non-negative matrix factorization has also been used to decompose matrices of code counts into small numbers of coarse signatures [52, 53]. Our work differs from these in the use of probabilistic independence as a guiding principle and the larger scale of our analysis.

A common approach to phenotype discovery has been *hard clustering* [54–61], in which each patient is assigned to exactly one cluster, using various measures of patient similarity and cluster quality, with salient clinical patterns then extracted from each cluster [62]. Hard clustering is appropriate when each record legitimately belongs to exactly one cluster, such as when grouping geographic locations or inferring disease subtypes that are truly disjoint. However, it fails when trying to identify signals that are better described as attributes, where each patient expresses varying levels of multiple attributes simultaneously [63]. When misapplied to that case, hard clustering tends to result in strong attributes overwhelming the more subtle attributes, which wind up distributed and obscured among the clusters. In medical records data, strong attribute signals can be demographics, common conditions unrelated to the disease of interest, or even which inclusion criteria brought the record into the dataset.

Contributions In this work we make the following contributions. First, we demonstrate a scalable approach for transforming episodic clinical data into continuous, longitudinal probabilistic curves. We apply the approach to the data modes of clinical measurements, medication mentions, demographics, and condition billing codes, each of which has unique behaviors and properties. Second, we demonstrate the use of the principle of probabilistic independence for large-scale disentangling of clinical signatures. Third, we evaluate the predictive power of the learned signatures by using their expression levels to predict the malignancy of solitary pulmonary nodules, and we assess the stability of our findings under different random seeds

for training. Finally, we investigate the learned signatures’ interpretive power by using them to understand the origin of the pulmonary nodules in the cohort.

2 Results

2.1 Inference Pipeline

The inference pipeline included data collection, transformation, and signature discovery components (Figure 1). The pipeline is summarized here, with detailed descriptions in the Methods section.

Data Collection We used two datasets drawn from our EHR: a *Discovery Set*, comprising 269,099 records of patients with a broad range of lung disease, used to learn the latent clinical signatures; and an *Evaluation Set* comprising 13,252 records of patients with no history of cancer preceding the discovery of a solitary pulmonary nodule, used to train and test the predictive model. The Evaluation Set is a subset of the Discovery Set.

We extracted 9195 variables from all records, including clinical measurements, billing codes, medication mentions, and demographics. Records in the evaluation set were labeled positive for patients who developed any lung malignancy over the 3 years after the nodule appearance, and negative for patients who did not (Table 1). 2651 records (20%) of the Evaluation Set were randomly partitioned into the final test set.

Data Transformation First, data were converted from episodic point observations to continuous longitudinal curves with a specific transformation for each data mode, where the transformation was a scalable approximate version of the more complex but principled transformation mentioned in the introduction. Clinical measurements were fit with a smooth interpolation that maintains non-stationarity, or a constant population median if a patient had no observations of a given test. Billing codes were represented as a longitudinal intensity curve of code occurrence events per unit time. Medication mentions were transformed to piecewise-constant 0/1 curves representing the presence or absence of the medication in a record at a given date. Demographics were represented as constant 0/1 curves, dummified from categorical variables when appropriate.

Next, curves for each patient were time-aligned and stacked, with cross sections sampled uniformly at random at a density of 1 sample per 3 record-years. An individual record may be randomly sampled once, more than once, or not at all, with longer records tending to be sampled more times. All sampled cross sections were stacked into a final data matrix of 630,000 rows by 9195 columns. Each column (corresponding to a single variable or *channel*, such as a specific laboratory test or billing code) was standardized to place them all onto

Attribute	Discovery Set	Labeled Evaluation Set	
		Malignant	Benign
Number of records	269,065	767	12,485
Male sex	144,258 (53.6%)	371 (48.4%)	5,728 (45.9%)
Female sex	124,793 (46.4%)	396 (51.6%)	6,757 (54.1%)
White race	202,553 (75.3%)	674 (87.9%)	10,126 (81.1%)
Black race	36,814 (13.7%)	63 (8.2%)	1,512 (12.1%)
Unknown race	17,338 (6.4%)	13 (1.7%)	449 (3.6%)
Other race	12,360 (4.6%)	17 (2.2%)	398 (3.2%)
Age (years)	52 [16,68]	68 [61,74]	59 [47,68]
Per Record			
Length (days before SPN event)	1,911 [407,4348]	1,707 [90,4057]	2,252 [406,4429]
Number condition codes	81 [27,224]	37 [11,125]	57 [22,149]
Number laboratory results	210 [41,764]	87 [14,430]	139 [39,464]
Number medication mentions	2 [0,28]	6 [0,50]	4 [0,35]
Unique condition codes	36 [16,71]	24 [10,51]	32 [16,61]
Unique laboratory tests	62 [14,94]	52 [7,77]	62 [23,86]
Unique medications	1 [0,7]	3 [0,9]	2 [0,8]

Table 1: Data summary statistics. Per record values are Median [IQI]. SPN = Solitary Pulmonary Nodule billing code.

roughly the same scale.

Clinical Signature Discovery The matrix \mathbf{X} of stacked cross sections was decomposed by FastICA [30] into $\mathbf{X} = \mathbf{AS}$, where the rows of \mathbf{S} are mutually independent, column $A_{\bullet i}$ represents the learned clinical signature of latent source i , and matrix element S_{ij} represents the level at which cross section $X_{\bullet j}$ expresses source i . The Direct LiNGAM method [33] is generally a more accurate method for performing this decomposition [13], in part because of the risk of ICA finding a local minimum, but it is far too inefficient for the matrix size used here.

ICA produces source expressions as rows $S_{i\bullet}$ that are centered at zero, but arbitrarily ordered and scaled. We re-scaled each row $S_{i\bullet}$ by dividing by two standard deviations, so that roughly 95% of the values in each $S_{i\bullet}$ are in $[-1, 1]$, and inversely scaled the corresponding column $A_{\bullet i}$ to maintain the invariant product. But because most of the $S_{i\bullet}$ are extremely sparse, peaky distributions, and the standard deviation depends on the degree of sparsity/peakiness, the scaling of the expressions is not strictly comparable between different signatures.

Clinical Signature Evaluation Signatures were evaluated subjectively for clinical coherence, and objectively by measuring how well they predict the lung malignancy label in

the Evaluation Set. Elastic Net, Random Forest, and Gradient Boosted Tree (XGBoost) architectures were trained for the malignancy prediction, one model of each using signature expressions \mathbf{S} and another model of each using original channel values \mathbf{X} as input. Optimal hyperparameters were determined independently using cross validation for each of the six models, then training on the full training set and testing on the held-out test set was repeated with 100 different random seeds each to determine the extent of variation due to randomness in training. Shapley values [36, 37] were used to interrogate each model for variable importance, and top predictors were evaluated for the explainability they provide.

2.2 Learned Clinical Signatures

Signatures of 2000 latent sources were computed and evaluated using the inference pipeline. Under informal expert review, the learned signatures appear clinically coherent, representing identifiable clinical pictures, including rare ones (Figure 3). The exact proportion of incoherent signatures was not quantified, and would be subject to disagreement on what constitutes incoherent, but subjectively the fraction of incoherent signatures appears to be small. (Signatures for all 2000 latent sources are given in supplemental material.) The algorithm assigns only a sequential identifier to each signature, but for ease of exposition, we have assigned descriptive names to those relevant to the discussion.

Signatures identify a quantitative pattern of changes to the record made by a given latent source. These signatures are extremely sparse, with the vast majority of the 9195 variables indicating standardized changes near zero for a given source. Our visual representation sorts the changes to all variables and presents those with an effect greater than a minimum threshold, or the top 10 affected variables, whichever is larger. In Figure 3, we interpret the signature as a relatively rare condition of Spasmodic Torticollis, a specific form of Dystonia. Quantities in parenthesis give the effect in original data units of a one-unit increase in expression of the source. For the `Abnormal involuntary movement` code, this is given as a factor 1.07, or a 7% increase in the code intensity. If the expression level were 10.0 (which from the inset histogram we can see occurs in around 100 of the samples in the Discovery Set), then this would correspond to code intensity increase by a factor of $1.07^{10.0} = 1.96$. The signature also specifies a slightly increased probability that the patient is `female` (increased by $0.006 \times 10 = 0.06$ for an expression of 10.0) or `white race`, and an increased probability that the patient is treated with `baclofen`, `clonazepam`, `gabapentin`, or `levodopa`. All of these align with what is known about the condition. Botulinum toxin, which is also used to treat the condition, is omitted here because it fell below the prevalence threshold for our input data, and so was not included in the analysis.

A second example is shown in Figure 4. This is for a much more sparsely expressed source, which we interpret as `Idiopathic pulmonary fibrosis` treated with `pirfenidone`.

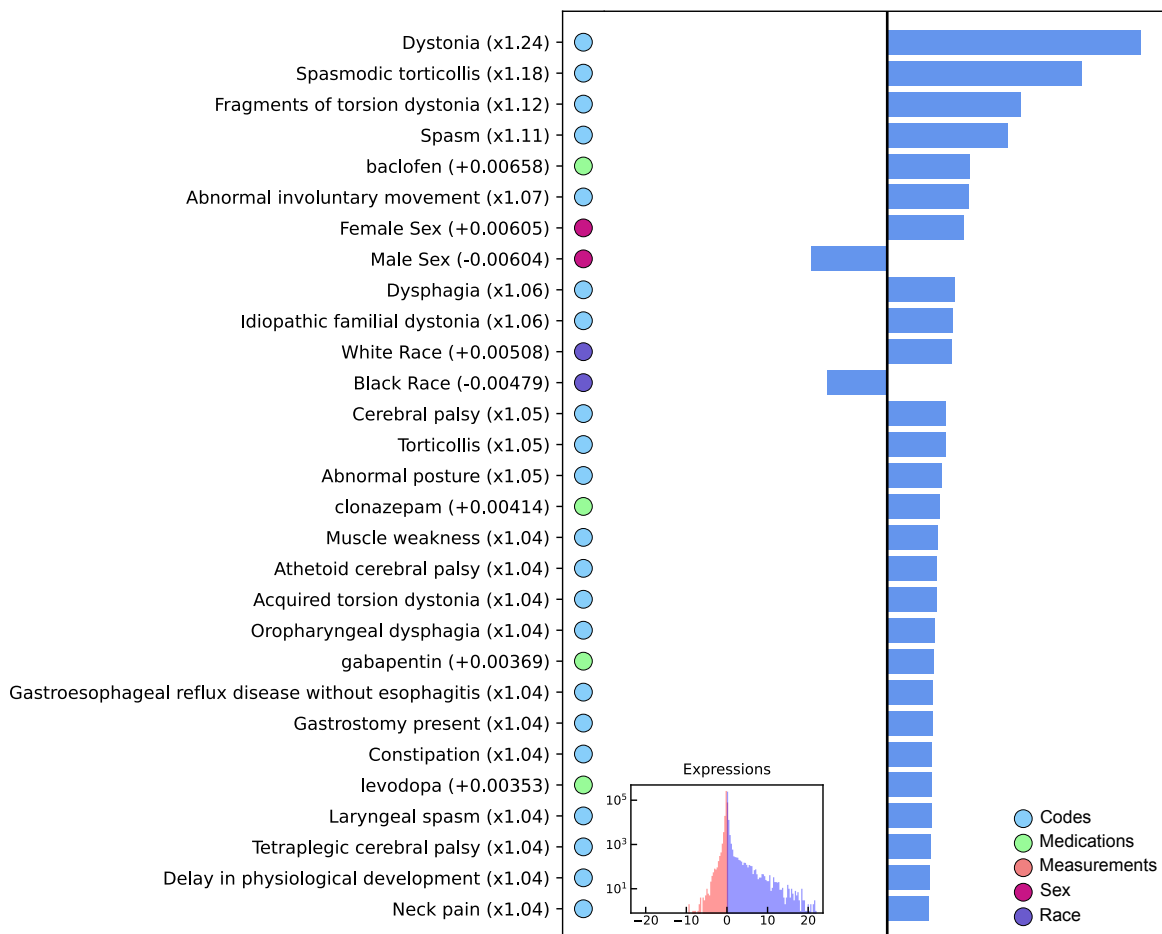


Figure 3: An example clinical signature, selected to illustrate the recovery of low-prevalence sources (here, a few hundred out of 630,000 sampled cross sections), and not cherry-picked for clinical coherence. We interpret this signature as representing the rare condition Spasmodic Torticollis [64], a specific type of dystonia. Bar length gives the size of the change in a given standardized variable, with numbers in parentheses indicating the change in original data units for a 1.0 change in expression. Changes may be either multiplicative ($\times \dots$) or additive ($+\dots$). Inset is a log-scaled histogram of expression levels in the Discovery Set sample matrix. Expression units are individually scaled for each signature such that the standard deviation is 0.5, placing 95% of all expressions within the interval $[-1, 1]$.

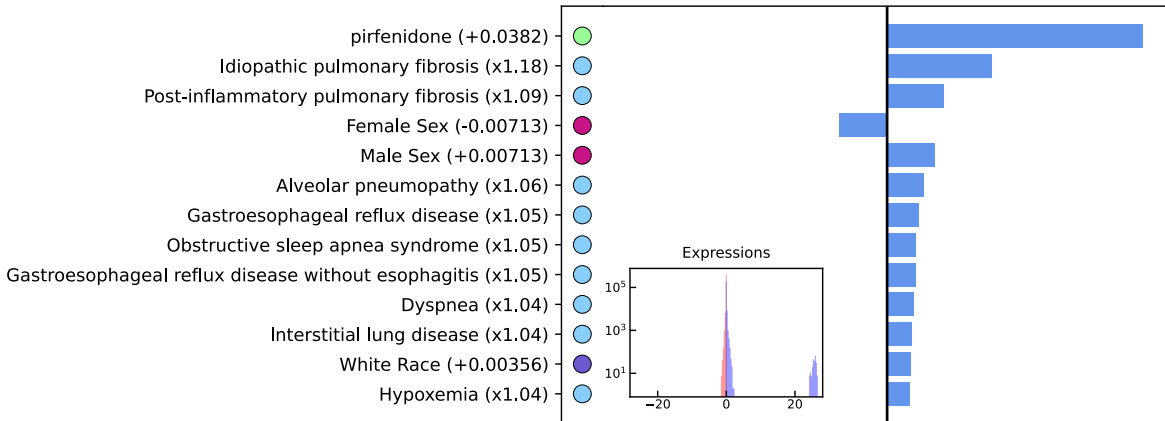


Figure 4: A second example signature of a rarely-expressed source, which we interpret as **Idiopathic pulmonary fibrosis** that is treated with **pirfenidone**. Several other signatures relate to this same condition without the treatment.

The source is meaningfully expressed only in some tens of cross sections, all of them with expression levels around 25. The signature is dominated by the **pirfenidone** treatment (with a $0.0382 \times 25 = 0.96$ probability increase of the medication appearing in the record), and includes the known (but incompletely understood) comorbidities of **Gastroesophageal reflux disease** and **Obstructive sleep apnea syndrome**. Not shown are five other signatures that include **Idiopathic pulmonary fibrosis**, one (1611, see Supplemental material) that looks like the common clinical picture, one (467) that explicitly distinguishes **Idiopathic pulmonary fibrosis** from **Post-inflammatory pulmonary fibrosis**, and three (674, 1113, 1957) that include it as a lower-probability element of a more general picture.

2.3 Lung Malignancy Prediction

Models that used signature expressions \mathbf{S} as input performed uniformly better at malignancy prediction than those that used the original data \mathbf{X} (Figure 5), suggesting that the signatures captured additional statistical strength from the larger Discovery Set, despite the fact that there were fewer of them (2000 signatures vs. 9195 variables).

Perhaps more important than the improved performance of the signatures as an input representation is the improved explanatory power they provide. We use the Random Forest results to illustrate, but the general conclusion holds for all models.

The top three predictive signatures for the Random Forest were signatures of malignancy in different locations of the respiratory tree (Figure 6), which makes sense from a causal perspective, but there is an interesting twist that suggests that they represent undiagnosed disease. The signatures include as dominant elements billing codes for cancer in various parts of the respiratory tract. The signatures were learned from the Discovery Set, which included

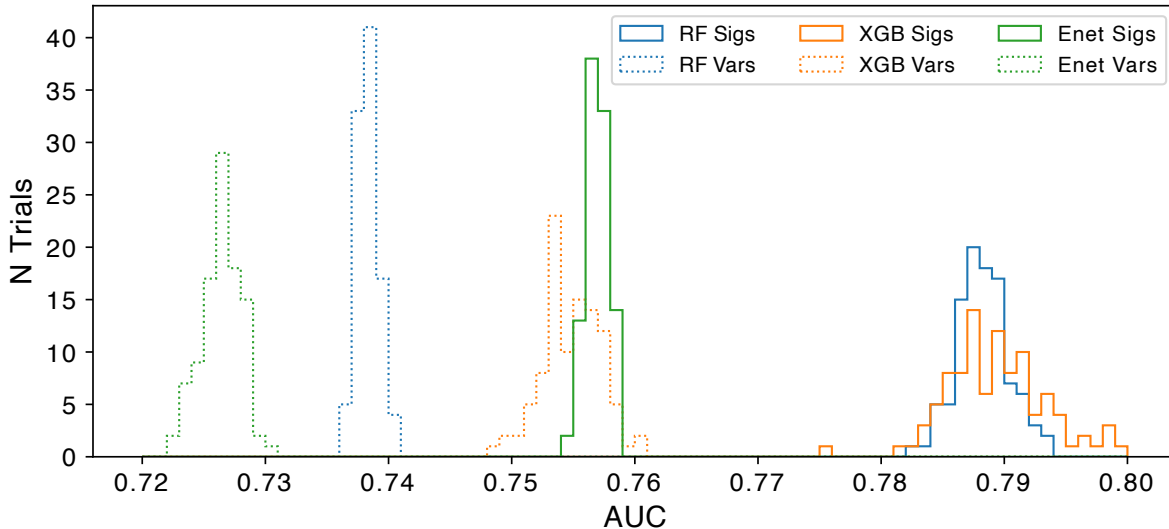


Figure 5: Histograms of area under the ROC curve (AUC) on the held out test set for all six models, each retrained 100 times with different random seeds. Models using the learned signatures \mathbf{S} (solid lines) were more predictive than those using the observed data matrix \mathbf{X} (dotted lines). Model variability solely due to the choice of random seed was substantial, especially for the XGBoost models. Median performance is a more robust indicator of performance; extremes in the tails are unlikely to generalize to unseen data [65].

records of many patients with diagnosed disease that contained such codes. However, the Evaluation Set was defined to include only patients with *no history of any type of cancer* before the pulmonary nodule was discovered, so no record in that set contained any cancer codes. Nevertheless, the remaining pattern of these signatures, even with the cancer codes absent in the patient record, turned out to be sufficiently sensitive that they were important predictors of malignancy, suggesting that at least some of these records were presenting undiagnosed disease. In practical application, high-magnitude expression of these signatures for a given patient record could prompt a search for the relevant malignancy, even before a solitary nodule appeared on imaging.

The fifth most predictive signature was primary bladder cancer (1452, Supplemental information), with the same reasons to believe that the model picked up undiagnosed disease. In this case, it suggests that the lung nodule in these patients is a metastasis from the bladder.

The most predictive latent sources identified by the three architectures were all informative and plausible (Figure 7), although the models disagreed on specifics of source importance and ranking. In contrast, the top predictors for models trained on the original data \mathbf{X} (Figure 8) did not produce actionable insights. Those top predictors include Age, COPD, Hypertension, and Tobacco Dependence, all of which are known strong associations, but none of them is anywhere near as acutely treatable as a signal of undiagnosed cancer.

The intensity of the **Solitary nodule of lung** code in a record (Figure 8) was a top



Figure 6: The top 3 predictive signatures in the Random Forest model. We interpret these as representing undiagnosed lung cancer for this dataset. Light-shaded bars are condition codes for lung malignancy that were present in Discovery Set records, but any record in which these codes occurred before the first solitary lung nodule code was deliberately excluded from the Evaluation Set. The fact that these signatures were top predictors for malignancy in that set, despite these missing malignancy codes, suggests that the remaining pattern in the signature was sufficiently sensitive for malignancy that any patients expressing them had undiagnosed cancer.

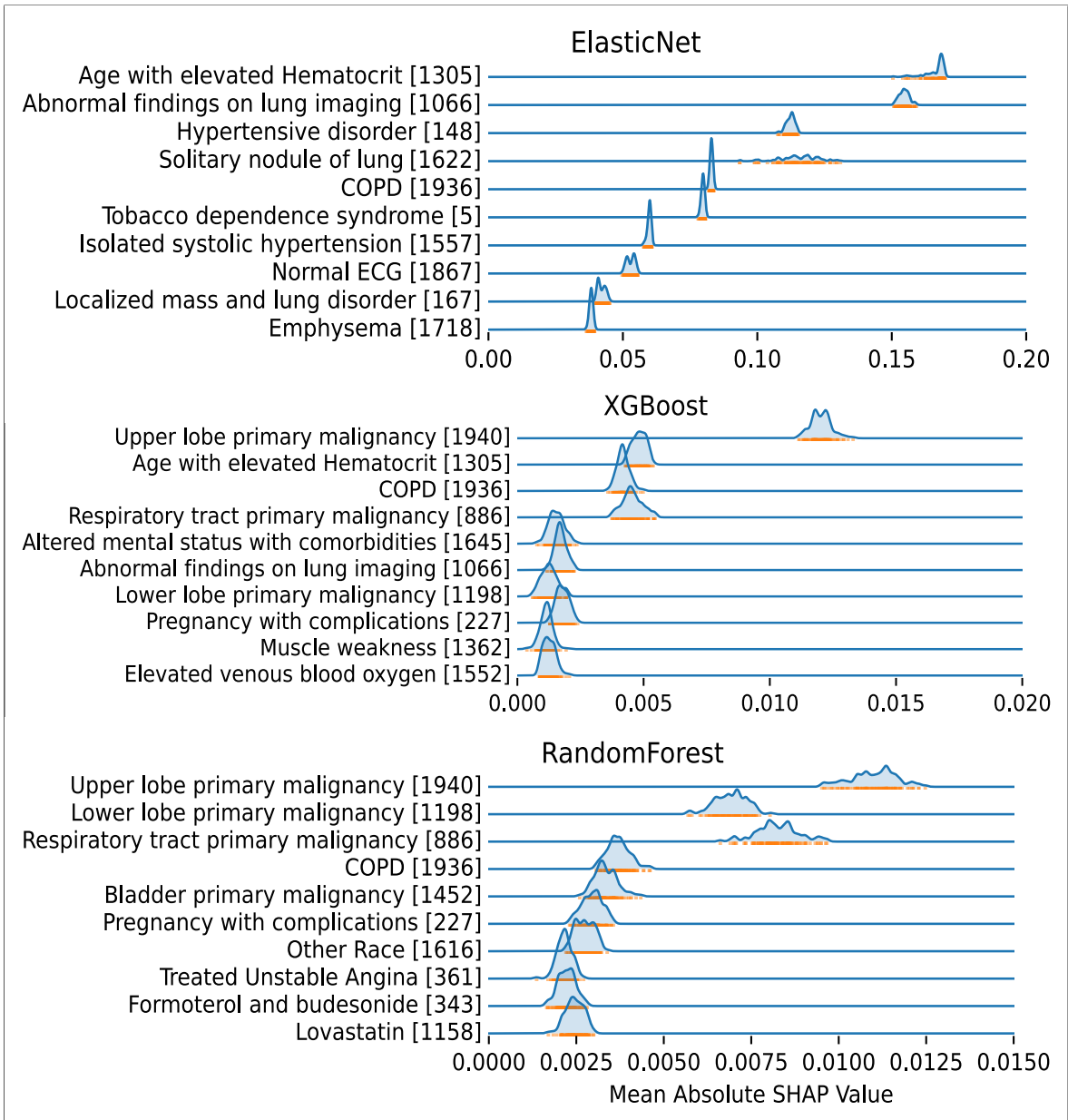


Figure 7: Predictive importance of the top 10 learned signatures. These are distributions over 100 different training random seeds for the optimal hyperparameter configuration of each architecture. Row order is by rank within the best of the 100. Numbers in brackets are the signature identifier in the supplementary material.

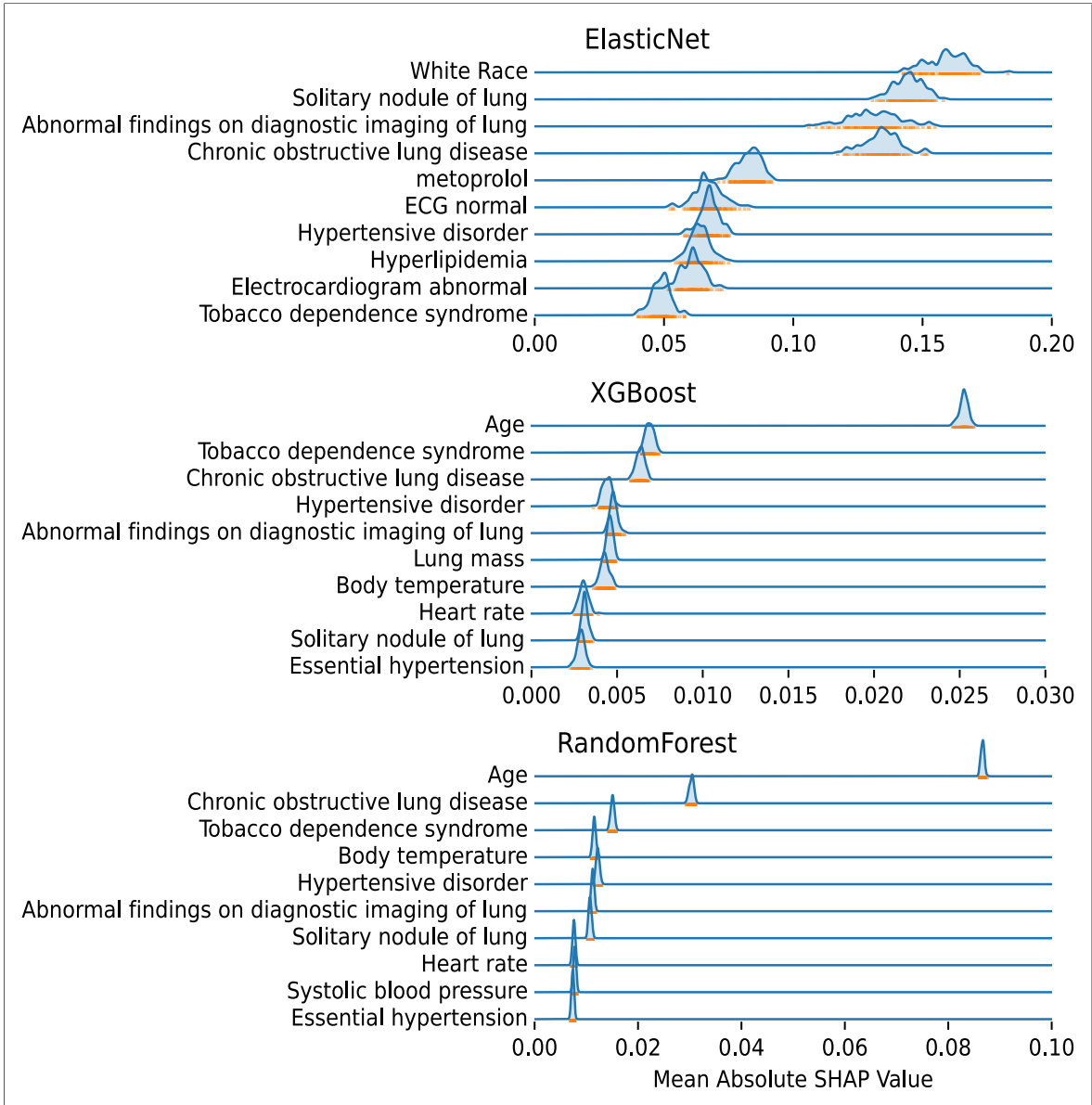


Figure 8: Predictive importance of the top 10 original variables. These are distributions over 100 different training random seeds for the optimal hyperparameter configuration of each architecture. Row order is by rank within the best of the 100.

predictor in the raw-variable models that, due to how the Evaluation Set was constructed, represented the length of the record preceeding the first event of that code. Specifically, each record in the set has exactly one instance of that code, because that was an inclusion criterion, and each record was truncated on the date of that code. The curve builder in our pipeline computed the time-intensity of all codes, which is usually a time-varying curve, but when any code had a number of events $m < 3$ in a given record of length l , our curve builder computed a constant value m/l for the full curve. Thus, the intensity for this channel became a constant $1/l$ for each record, and record length is clearly distributed differently between positive and negative cases (Table 1). This would have represented an information leak had the length of the record been calculated to include future data beyond the first nodule code, but that wasn't the case here. Instead, this variable represents a (probably site-specific) process signal [66] encoding the fact that patients who turn out to have a malignant nodule tend to have a shorter history at our institution than patients who turn out to have a benign nodule.

3 Discussion

We have described an unsupervised method of using probabilistic independence to disentangle from EHR data the clinical signatures of multiple, simultaneously expressed sources of disease. This includes a method to transform the noisy, sparse, and irregular EHR data of multiple different data modes (billing code events, medication mentions, clinical measurements, and demographics) into dense, regular data that can be operated on by standard machine learning methods.

We demonstrated that a given patient's expression \mathbf{S} of the latent sources is more predictive for lung cancer than the dense matrix \mathbf{X} of original variables, which implies that the signatures are capturing meaningful clinical patterns, and may be transferring some statistical strength from the large unlabeled Discovery Set to the smaller labeled training set.

We investigated the clinical utility of the learned signatures in explaining the models' predictions and in understanding the pathophysiologic sources of the predicted lung cancer in patients with a documented solitary lung nodule. We found that the top predictors display clinical face validity, and help to understand the causes of malignancy of a given nodule; in this case there is evidence that the most important causes are previously undiagnosed cancer, either in the lung or other organs.

Our methods can be extended to include other data sources. In particular, concepts extracted from progress notes, panomics data, environmental exposures, and personal sensors could be added to give richer, higher-resolution signatures without modifying the underlying algorithms.

While in theory we expect the predictors in \mathbf{S} to reflect root causes of disease, in practice

we found important differences in how the S_i were used between Elastic Net, Random Forest, and XGBoost models (Figure 7), which urges caution in drawing causal conclusions. We speculatively attribute the performance difference (about 0.03 AUC) between the linear and tree ensemble models to residual interactions between the S_i and their potential nonlinear relationship to Y , both of which can be modeled better by tree ensembles.

From our perspective, the Random Forest results look clinically the most plausible. We hypothesize that the broader and more random search performed by Random Forest training may have produced a more representative model, while the greedy XGBoost approach may be more likely to find local minima. Some evidence for this interpretation lies in the disproportionately dominant use by XGBoost of `Upper lobe primary malignancy`, the most common location for lung malignancies. The $10\times$ higher Shapley values for the top XGBoost predictors also suggests that the algorithm is anchoring on just a few strong sources, as we might expect from a greedy algorithm. Understanding these differences is a direction for future study.

In addition to the variation in the learned structure, the random variation of discrimination performance was higher than anticipated. The range of AUC under random-seed variation was about 0.02 for the gradient-boosted tree classifier, 0.01 for the random forest, and 0.005 for the elastic net (Figure 5). This variation was larger than we expected, typically at least as large as the change due to a hyperparameter adjustment during tuning, which could easily mislead an algorithmic search for the best hyperparameters. In our experience, sequential model-based optimization strategies such as those using Bayesian Optimization [67, 68] can be fooled by randomness this large into settling on non-optimal settings, even though the optimization algorithms are designed to handle some amount of noise. In contrast, random search is non-sequential, allowing one to identify an optimum by eye, after the trials are run. So while sequential optimization can produce superior models under a given tuning budget, in practice the benefit may depend on the degree of variation in performance due to the random seed.

The variation under random seed selection also urges caution with the increasingly common practice of trying many random seeds and then accepting the best performing model to report. If the goal of a project is to find the single best performing model for a given purpose (such as for a competition or a purpose-built model for deployment), then random-seed hunting can be a useful practice. But if the goal is to evaluate a *given architecture* or a *given set of predictive variables*, or to understand whether a *given learning approach* produces better results than some alternative (a common goal in the machine learning literature, and our goal here), then seed hunting can produce invalid conclusions, because the effect of the random seed can overshadow or even reverse the actual performance increment produced by the idea being tested.

Moreover, seed hunting may backfire when there is any out-of-distribution (OOD) compo-

ment of the application, such as when the model is deployed at a different time or at a different institution from where it was trained [65]. Our results demonstrate that different random seeds can produce meaningfully different model structure. This variation may either help or hurt when applied to slightly OOD data, and it is difficult to predict in which direction that will go [65].

Limitations In this work we do not demonstrate that any of the predictive algorithms recover the truth about the source of a given patient’s disease, and the fact that the three models disagree on the global results demonstrates that at least two of them are incorrect in many cases. Establishing truth, and investigating the effect of model architecture on the recovery of that truth, would require a large-scale synthetic data experiment, and is a direction for future work. Previous experiments in the domain of liver failure, however, produced results that closely align with what is known about the disease [10].

We use binary variables for medications and demographics, and interpret the quantities that represent them in signatures as probabilities. This seems to work reasonably well, despite the fact that the ICA decomposition $\mathbf{X} = \mathbf{A}\mathbf{S}$ is defined only for continuous-valued variables. There is evidence suggesting that binary observations may be used without algorithm modification if the observations are sparse (mostly zero) or the latent sources are sparse (mostly near zero) [69]. In our case, the medication variables are sparse, as are nearly all of the latent sources.

Finally, latent signatures \mathbf{A} are not likely to be transportable, because the probabilities represented in them capture site-specific practices that are not likely to be reproduced at a different institution, or even by the same institution over time [66]. However, to the extent that the signatures capture latent sources that are intrinsic to disease states, rather than operational practice patterns, the *expressions* \mathbf{S} of the latent sources may play a role in transportability, despite their signatures differing across sites.

Conclusion We have demonstrated large-scale, data-driven inference of latent disease sources, using routinely collected, multi-modal EHR data. The method recovers coherent, clinically recognizable signatures or patterns of pathophysiologic changes caused by those sources, including some found in less than one in 10^4 training instances. The signatures cover a broad range of disease, and provide intuitive dimensions for understanding a patient record. In a lung cancer prediction task, they outperformed the original observed variables as inputs, and suggested clinically undiagnosed malignancy as top predictors.

4 Methods

This research was approved as non-human-subjects research by the Vanderbilt University Institutional Review Board (#210761).

4.1 Data

All data were extracted from the research mirror of VUMC’s EHR, which covers about 3 million patients, with nearly all inpatient and outpatient records complete after 2005. HIPAA-defined Personal Health Information (names, record numbers, absolute dates, etc.) was removed before processing.

Original ICD-9 and ICD-10 billing codes were mapped onto the SNOMED condition code taxonomy, original medications were resolved into ingredients, and extreme values for clinical measurements that were deemed impossible or incompatible with life were removed. Any resulting variables with fewer than 1000 total observed instances in the database were excluded, and measurements present in fewer than 10 records of the Discovery Set (see below) were excluded. A final total of $p = 9195$ variables were recorded, including 7453 SNOMED condition codes, 771 medication ingredients, 949 clinical measurements, and 12 demographics (1 age continuous variable, 3 sex categories, and 8 race categories). Categorical variables were dummified into binary variables.

4.1.1 Discovery Set

A set of 95 condition concepts was curated by a pulmonologist to include a broad scope of infectious, malignant, and other lung conditions. Patient records were included in the Discovery Set if they contained at least one billing code descended from any of the concepts prior to the cutoff date of 4/29/2022. Records were excluded if they contained fewer than two distinct dates containing an observation of a condition, measurement, or medication. A total of 269,099 records met these criteria.

4.1.2 Evaluation Set

A cohort of 13,252 records was collected comprising those with at least one billing code for a solitary pulmonary nodule (SPN), and no codes for any type of malignancy preceding the SPN date. Because the code for an SPN was among the lung condition codes defining the Discovery Set, the Evaluation Set was a subset of the Discovery Set.

Evaluation Set records were labeled positive if they contained at least one code for a malignant lung neoplasm (including primary lung cancer or metastasis from other locations) on day 4 - 1095 following the SPN date. Records were labeled negative if they had no lung malignancy code before day 1095, even if they had a malignancy in some other organ after the

SPN date. Records with lung malignancy codes within 4 days of the SPN code were excluded because they represented cases where the malignancy status was presumed to be known at the time of the SPN detection. Labels were validated by comparison with cancer registry records (all positive labeled records) and manual chart review (all mismatches with the cancer registry and a random sample of negative labeled records) as detailed elsewhere [70], and estimated to have 0.98 PPV, 0.99 NPV, 0.93 sensitivity, and 0.996 specificity.

A random partition of 2651 records (20%) of the Evaluation Set were set aside as the final test set.

4.2 Continuous Curve Generation

Continuous longitudinal curves were built with methods specific to each data mode. A curve was generated for each *channel* (corresponding to a single clinical variable, such as a specific laboratory test or billing code) with one-day resolution. The time constant of the actual information captured by the curve was usually not as small as one day, because observations were made in general at far larger intervals. Nevertheless, creating the longitudinal curves at this resolution allows us to estimate the value of a given variable on arbitrary dates, given the set of observations.

4.2.1 Clinical Measurements

Curves for clinical measurements (mostly laboratory test results) were originally built using non-stationary Gaussian process regression [12], which provides a distribution over all possible paths that the measurand could have taken over time, given the observed values and assumptions on the smoothness of the path. However, that method is too inefficient for large-scale use. For this work, we used the univariate PCHIP method [71] that interpolates a curve with a continuous first derivative through all observations. This method adapts to non-stationarity, maintains monotonicity given monotonic data, and does not overshoot the maxima defined by the observations. Extrapolation beyond the first and last observation used the value of the nearest observation.

If a record listed no observations for a given clinical measurement, a constant curve at the population median was imputed.

4.2.2 Billing Codes

Curves for billing code events were originally computed as the intensity curves of non-homogeneous gamma processes [11], which provide a distribution over all possible intensity curves, given smoothness assumptions, as well as a distribution over a shape parameter that models dependence between adjacent events.

To trade approximation for complexity with this data mode, we replaced the gamma process with a simple density function that assumes memorylessness between events, but is still able to model nonstationarity over time. Specifically, we used a variation we developed for Random Average Shifted Histograms (RASH) [72]. RASH estimates an intensity curve by averaging many equally-spaced histograms over the data, with each histogram shifted by a random amount. It produces a smooth curve similar to kernel density estimation (KDE), but the constant bin width causes the same problems with nonstationarity that a constant KDE bandwidth causes. To accommodate nonstationarity, we modified RASH to use random-sized bins, with the random choice of bin size made in event space rather than data space. For example, a bin size of 5.7 would mean that the bin includes the next 5 events plus 70% of the interval between the 5th and 6th events. Bins were specified in increasing order by event time, with each bin size chosen uniformly at random between 3.0 and the number of remaining events. This naturally handles the non-stationarity in event density, with events spaced further apart in time allocated into wider time bins than events closer in time.

4.2.3 Medication Mentions

Curves for medication mentions were binary curves intended to reflect whether the patient had been prescribed to take the medication at the indicated time. Creating the curve was challenging, however, because for much of the history of our EHR, the start and stop dates of medications are either missing or unreliable, and dispensing or refill data was not available. Instead, at some patient visits, a clinician would review the current medication list with the patient, confirming or removing entries. The modified list was then inserted into the database and marked with the date of the reconciliation.

Curves were computed by setting them at 1 (taking) for all medications mentioned on a given reconciliation, and 0 (not taking) otherwise. Times between reconciliations used the value of the nearest observation.

If a record included no mentions of a given medication, a constant curve of 0 was imputed.

4.2.4 Demographics

Curves for demographics were either constant (race, sex) or linearly increasing (age). Categorical values were dummified into sets of binary curves.

4.2.5 Smoothing

We found that capturing a small amount of history in the curves was useful for capturing short-term trajectories of disease and filling short documentation gaps. To do this, a one-year retrospective rolling mean was applied to each curve. For medications, the ‘taking’ region of each curve was extended for 365 days in each direction.

4.3 Cross-section Sampling

All curves from the i^{th} record were aligned into a curveset, anchoring on the first date of the record. A number c_i of cross-sections were sampled uniformly at random from each record in the Discovery Set, where $c_i \sim \text{Bin}(l_i, d)$, l_i is the record length in days and the sampling density $d = 1/(3 * 365)$ was fixed at one sample per three record-years. Longer records therefore had a higher probability of being sampled multiple times, and some records were not sampled at all. A total of $n = 630,037$ cross sections from 175,711 records were sampled and stacked into the matrix $\mathbf{X} \in \mathbb{R}^{p \times n}$. The size of \mathbf{X} (controlled by sampling density d) was limited by available RAM and the need for the FastICA implementation to hold multiple copies of intermediate matrices in memory at once.

In the Evaluation Set, records were sampled exactly once, at the time of the first SPN billing code. No data observed after the SPN date were used to construct the curves for the Evaluation Set.

4.3.1 Standardization

The discovery matrix \mathbf{X} was transformed to bring variables from all modes onto roughly the same scale. Different transformations were used for different row subsets that correspond to data modes.

The row subset $\mathbf{X}^C = \mathbf{X}_{i\bullet}, i \in V^C$ of clinical measurement variables V^C and the row subset $\mathbf{X}^M = \mathbf{X}_{i\bullet}, i \in V^M$ of medication variables V^M were each transformed by subtracting the subset mean and dividing by two standard deviations.

The row subset $\mathbf{X}^B = \mathbf{X}_{i\bullet}, i \in V^B$ of billing code intensity variables V^B was first transformed to $\tilde{\mathbf{X}}^B = \log(\mathbf{X}^B + \epsilon)$, where the smoothing value $\epsilon = 1/(20 \times 365)$ represents an arbitrarily chosen prior of one code per twenty record-years, and then each row $\tilde{\mathbf{X}}_{i\bullet}^B$ was scaled by dividing by $s = 2 \cdot \text{std}(\tilde{\mathbf{X}}_{i\bullet}^B)$.

Demographics were not transformed, remaining as 0/1 variables.

The logarithmic transform affects the composition of the signatures and their expression values, but the scaling operations only affect the relative ranking of the different data modes in the signature visualizations.

Evaluation set cross sections were standardized using the transformation determined by the Discovery Set.

4.4 Clinical Signature Discovery

The final discovery matrix $\mathbf{X} \in \mathbb{R}^{p \times n}$ was decomposed by ICA [30,31] into a mixing matrix $\mathbf{A} \in \mathbb{R}^{p \times k}$ and a source matrix $\mathbf{S} \in \mathbb{R}^{k \times n}$, such that $\mathbf{X} = \mathbf{AS}$, the rows of \mathbf{S} are (close to) mutually probabilistically independent, and k is the number of latent sources inferred. In

terms of our application, the column $X_{\bullet j}$ is the j^{th} sampled cross section, column $A_{\bullet i}$ is the clinical signature of latent source i , and matrix element S_{ij} represents the level at which cross section $X_{\bullet j}$ expresses source i .

Mathematically, we can infer $k = p$ components, although optimally, we want to match k to the intrinsic dimension of \mathbf{X} to avoid over- or under-learning [30]. In our case, we used $k = 2000$. We suspect that the optimal $k > 2000$, but we were limited by the computational complexity of the algorithm and the need for the scikit-learn implementation to maintain multiple intermediate matrices in RAM. To infer $k < p$, standard implementations use the modified ICA equation $\mathbf{VX} = \mathbf{AS}$, or $\mathbf{X} = \mathbf{V}^{-1}\mathbf{AS} = \tilde{\mathbf{A}}\mathbf{S}$, where $\mathbf{V} \in \mathbb{R}^{k \times p}$ is obtained from singular value decomposition and provides the additional benefit of whitening the data [30]. In this paper, when we refer to our computed results as \mathbf{A} , we are technically referring to this $\tilde{\mathbf{A}}$.

The matrix \mathbf{X}^E of the Evaluation Set was created analogously to the discovery matrix \mathbf{X} , with the exception of each record being sampled exactly once. The same standardizing transformations were applied (with the same parameters) as with the Discovery Set. Evaluation Set source expressions $\mathbf{S}^E = \tilde{\mathbf{A}}^{-1}\mathbf{X}^E$ were computed, and the matrices \mathbf{S}^E and \mathbf{X}^E were partitioned into training and test sets, using the patient-level partitioning described above.

4.5 Clinical Signature Evaluation

First, the face validity of the clinical signatures were evaluated subjectively and informally, by examining the identified patterns and considering how well they represent recognizable patterns of disease. Next, they were evaluated objectively by measuring how well the expression matrix \mathbf{S}^E predicts the malignancy label Y in a Random Forest (Python 3.10, scikit-learn 1.1.3), a Gradient-Boosted Machine (Python 3.10, XGBoost 1.6), and an Elastic Net (Python 3.10, scikit-learn 1.0.2), compared to how well the observed variable matrix \mathbf{X}^E predicts Y with the same architectures. Hyperparameters for all six models were optimized independently using $10 \times$ cross validation using a combination of random search, grid search, and human guided search. After optimal hyperparameters were determined for each model, training on the full training set and testing on the test set were repeated with 100 different random seeds each to determine the extent of variation due to randomness in training.

Models were interrogated for variable importance using Shapley values [36,37], which estimate the contribution of each predictive variable, taking into account all possible interactions of that variable with others.

5 Acknowledgements

This work was funded in part by grant award CA253923 from the National Cancer Institute. It relied on data from the VUMC Research Derivative, supported by CTSA award UL1 TR002243 from the National Center for Advancing Translational Sciences. Its contents are solely the responsibility of the authors and do not necessarily represent official views of the National Center for Advancing Translational Sciences or the National Institutes of Health.

6 Competing Interests

The authors declare that there are no competing interests.

7 Author Contribution

Overall concept and direction by TAL. Unsupervised learning approach designed by TAL, WWS, EVS, JMS, and implemented by TAL, JMS. Supervised evaluation designed by TAL, BAL, FM, and implemented by JMS, TL, MBM. Analysis and interpretation of results by all authors. Manuscript draft by TAL, with critical revision by all authors. All authors take responsibility for the final manuscript contents.

8 Data Availability

The electronic health record data that support the findings of this study are available upon request from the corresponding author, approval from the institutions' respective IRBs, and approval from an additional VUMC representative assessing institutional risk. Requests for access will be processed within around 2 months, subject to signing a data use agreement.

9 Code Availability

Source code for this project is available at https://github.com/ComputationalMedicineLab/ipn_methods_code_public.

References

- [1] Anderson GP. Endotyping asthma: new insights into key pathogenic mechanisms in a complex, heterogeneous disease. *Lancet*. 2008 Sep;372(9643):1107–1119.

- [2] Ringman JohnM, Goate A, Masters ColinL, Cairns NigelJ, Danek A, Graff-Radford N, et al. Genetic heterogeneity in alzheimer disease and implications for treatment strategies. *Curr Neurol Neurosci Rep.* 2014;14(11).
- [3] Gutmann DH. Eliminating barriers to personalized medicine: Learning from neurofibromatosis type 1. *Neurology.* 2014 Jun;
- [4] Tuomi T, Santoro N, Caprio S, Cai M, Weng J, Groop L. The many faces of diabetes: a disease with increasing heterogeneity. *The Lancet.* 2014;383(9922):1084–1094.
- [5] Oksel C, Haider S, Fontanella S, Frainay C, Custovic A. Classification of Pediatric Asthma: From Phenotype Discovery to Clinical Practice. *Front Pediatr.* 2018;6. Available from: <https://www.frontiersin.org/articles/10.3389/fped.2018.00258>.
- [6] Gul ZG, Kaplan SA. BPH: Why Do Patients Fail Medical Therapy? *Curr Urol Rep.* 2019 Jun;20(7):40.
- [7] Schoettler N, Strek ME. Recent Advances in Severe Asthma: From Phenotypes to Personalized Medicine. *Chest.* 2020 Mar;157(3):516–528.
- [8] Wang Z, Huang J, Xie D, He D, Lu A, Liang C. Toward Overcoming Treatment Failure in Rheumatoid Arthritis. *Front Immunol.* 2021;12. Available from: <https://www.frontiersin.org/articles/10.3389/fimmu.2021.755844>.
- [9] Lasko TA, Denny JC, Levy MA. Computational phenotype discovery using unsupervised feature learning over noisy, sparse, and irregular clinical data. *PLoS One.* 2013;8(6):e66341.
- [10] Lasko TA, Mesa DA. Computational phenotype discovery via probabilistic independence. In: *Proc KDD Workshop Appl Data Sci Healthc. DSHealth*; 2019. .
- [11] Lasko TA. Efficient inference of Gaussian process modulated renewal processes with application to medical event data. In: *Proc. Thirtieth Conf. Uncertain. Artif. Intell. UAI*; 2014. Available from: <https://auai.org/uai2014/acceptedPapers.shtml>.
- [12] Lasko TA. Nonstationary gaussian process regression for evaluating clinical laboratory test sampling strategies. In: *Proc. Twenty-Ninth AAAI Conf. Artif. Intell. Proc Conf AAAI Artif Intell*; 2015. p. 1777–1783. Available from: <https://aaai.org/papers/456-nonstationary-gaussian-process-regression-for-evaluating-repeated-clinical-laborato>
- [13] Strobl EV, Lasko TA. Identifying patient-specific root causes of disease. In: *Proc. 13th ACM Int. Conf. Bioinforma. Comput. Biol. Health Inform. BCB '22.* New York, NY, USA: Association for Computing Machinery; 2022. p. 1–10.

- [14] Strobl EV, Lasko TA. Identifying patient-specific root causes with the heteroscedastic noise model. *Journal of Computational Science*. 2023 Sep;72:102099.
- [15] Strobl E, Lasko TA. Sample-Specific Root Causal Inference with Latent Variables. In: *Proc. Second Conf. Causal Learn. Reason.* PMLR; 2023. p. 895–915. Available from: <https://proceedings.mlr.press/v213/strobl123b.html>.
- [16] Barbero Mota M, Gamboa JL, Still JM, Stein CM, Kawai VK, Lasko TA. Pos0114 Computational Identification of Sle Patient Records Using Data-Driven Clinical Fingerprints. *Ann Rheum Dis*. 2022 Jun;81(Suppl 1):282–282.
- [17] Li TZ, Still JM, Xu K, Lee HH, Cai LY, Krishnan AR, et al.. Longitudinal Multimodal Transformer Integrating Imaging and Latent Clinical Signatures From Routine EHRs for Pulmonary Nodule Classification. *arXiv*; 2023.
- [18] Jolliffe IT. *Principle component analysis*. 2nd ed. Springer; 2004.
- [19] Abdi H, Williams LJ. *Principal component analysis*. *Wiley Interdiscip Rev Comput Stat*. 2010;2(4):433–459.
- [20] Strang G. Section 6.7: Singular Value Decomposition (SVD). In: *Introduction to linear algebra*. 3rd ed. Wellesley, MA: Wellesley-Cambridge; 2003. p. 352–362.
- [21] Blei DM, Ng AY, Jordan MI. Latent dirichlet allocation. *J Mach Learn Res*. 2003;3:993–1022.
- [22] Vincent P, Larochelle H, Lajoie I, Bengio Y, Manzagol PA. Stacked Denoising Autoencoders: Learning Useful Representations in a Deep Network with a Local Denoising Criterion. *J Mach Learn Res*. 2010;11(110):3371–3408. Available from: <http://jmlr.org/papers/v11/vincent10a.html>.
- [23] Masci J, Meier U, Ciresan D, Schmidhuber J. Stacked Convolutional Auto-Encoders for Hierarchical Feature Extraction. In: Honkela T, Duch W, Girolami M, Kaski S, editors. *Artif. Neural Netw. Mach. Learn. – ICANN 2011. Lecture Notes in Computer Science*. Berlin, Heidelberg: Springer; 2011. p. 52–59.
- [24] Doersch C. Tutorial on Variational Autoencoders. *arXiv*; 2021.
- [25] Chen RTQ, Li X, Grosse R, Duvenaud D. Isolating Sources of Disentanglement in Variational Autoencoders. *arXiv*; 2019.
- [26] Burgess CP, Higgins I, Pal A, Matthey L, Watters N, Desjardins G, et al.. Understanding disentangling in β -VAE. *arXiv*; 2018.

- [27] Mathieu E, Rainforth T, Siddharth N, Teh YW. Disentangling Disentanglement in Variational Autoencoders. In: Proc. 36th Int. Conf. Mach. Learn. PMLR; 2019. p. 4402–4412. Available from: <https://proceedings.mlr.press/v97/mathieu19a.html>.
- [28] Saelens W, Cannoodt R, Saeys Y. A comprehensive evaluation of module detection methods for gene expression data. *Nat Commun.* 2018 Mar;9(1):1090.
- [29] Sastry AV, Hu A, Heckmann D, Poudel S, Kavvas E, Palsson BO. Independent component analysis recovers consistent regulatory signals from disparate datasets. *PLOS Computational Biology.* 2021 Feb;17(2):e1008647.
- [30] Hyvarinen A, Oja E. Independent component analysis: Algorithms and applications. *Neural Netw.* 2000;13(4-5):411–430.
- [31] Hyvarinen A, Karhunen J, Oja E. Independent component analysis. New York: Wiley; 2001.
- [32] Shimizu S, Hoyer PO, Hyvärinen A, Kerminen AJ. A linear non-gaussian acyclic model for causal discovery. *J Mach Learn Res.* 2006;7:2003–2030. Available from: <http://jmlr.org/papers/v7/shimizu06a.html>.
- [33] Shimizu S, Inazumi T, Sogawa Y, Hyvärinen A, Kawahara Y, Washio T, et al. DirectLiNGAM: A direct method for learning a linear non-gaussian structural equation model. *J Mach Learn Res.* 2011;12:1225–1248. Available from: <http://dl.acm.org/citation.cfm?id=2021040>.
- [34] Hyvarinen A, Sasaki H, Turner R. Nonlinear ICA Using Auxiliary Variables and Generalized Contrastive Learning. In: Proc. Twenty-Second Int. Conf. Artif. Intell. Stat. PMLR; 2019. p. 859–868. Available from: <https://proceedings.mlr.press/v89/hyvarinen19a.html>.
- [35] Hyvarinen A, Khemakhem I, Morioka H. Nonlinear Independent Component Analysis for Principled Disentanglement in Unsupervised Deep Learning. arXiv; 2023.
- [36] Lundberg SM, Lee SI. A unified approach to interpreting model predictions. In: Guyon I, Luxburg UV, Bengio S, Wallach H, Fergus R, Vishwanathan S, et al., editors. *Advances in neural information processing systems* 30. Curran Associates, Inc.; 2017. p. 4765–4774. Available from: <http://papers.nips.cc/paper/7062-a-unified-approach-to-interpreting-model-predictions.pdf>.
- [37] Lundberg SM, Erion G, Chen H, DeGrave A, Prutkin JM, Nair B, et al. From local explanations to global understanding with explainable AI for trees. *Nat Mach Intell.* 2020 Jan;2(1):56–67.

- [38] Newton KM, Peissig PL, Kho AN, Bielinski SJ, Berg RL, Choudhary V, et al. Validation of electronic medical record-based phenotyping algorithms: results and lessons learned from the eMERGE network. *Journal of the American Medical Informatics Association*. 2013 Jun;20(e1):e147–e154.
- [39] Kirby JC, Speltz P, Rasmussen LV, Basford M, Gottesman O, Peissig PL, et al. PheKB: a catalog and workflow for creating electronic phenotype algorithms for transportability. *J Am Med Inform Assoc JAMIA*. 2016 Nov;23(6):1046–1052.
- [40] Chapman M, Mumtaz S, Rasmussen LV, Karwath A, Gkoutos GV, Gao C, et al. Desiderata for the development of next-generation electronic health record phenotype libraries. *GigaScience*. 2021 Sep;10(9).
- [41] Lasko TA. Inferring the latent intensity of clinical events using modulated renewal processes. In: *NIPS 2013 Workshop Mach. Learn. Clin. Data Anal. Healthc.*; 2013. .
- [42] Che Z, Purushotham S, Khemani R, Liu Y. Distilling knowledge from deep networks with applications to healthcare domain. *ArXiv Prepr ArXiv151203542*. 2015;.
- [43] Bajor JM, Mesa DA, Osterman TJ, Lasko TA. Embedding complexity in the data representation instead of in the model: A case study using heterogeneous medical data. *ArXiv Prepr*. 2018-02-12, 2018;abs/1802.04233.
- [44] Weng WH, Szolovits P. Representation Learning for Electronic Health Records. *arXiv*; 2019.
- [45] Darabi S, Kachuee M, Fazeli S, Sarrafzadeh M. TAPER: Time-Aware Patient EHR Representation. *IEEE J Biomed Health Inform*. 2020 Nov;24(11):3268–3275.
- [46] Steinberg E, Jung K, Fries JA, Corbin CK, Pfohl SR, Shah NH. Language models are an effective representation learning technique for electronic health record data. *Journal of Biomedical Informatics*. 2021 Jan;113:103637.
- [47] Si Y, Bernstam EV, Roberts K. Generalized and transferable patient language representation for phenotyping with limited data. *Journal of Biomedical Informatics*. 2021 Apr;116:103726.
- [48] Liu S, Wang X, Hou Y, Li G, Wang H, Xu H, et al. Multimodal Data Matters: Language Model Pre-Training Over Structured and Unstructured Electronic Health Records. *IEEE J Biomed Health Inform*. 2023 Jan;27(1):504–514.
- [49] Choi E, Xu Z, Li Y, Dusenberry M, Flores G, Xue E, et al. Learning the Graphical Structure of Electronic Health Records with Graph Convolutional Transformer. *Proc AAAI Conf Artif Intell*. 2020 Apr;34(01):606–613.

- [50] Pivovarov R, Perotte AJ, Grave E, Angiolillo J, Wiggins CH, Elhadad N. Learning probabilistic phenotypes from heterogeneous EHR data. *J Biomed Inform.* 2015 Dec;58:156–165.
- [51] Li Y, Nair P, Lu XH, Wen Z, Wang Y, Dehaghi AAK, et al. Inferring multimodal latent topics from electronic health records. *Nat Commun.* 2020 May;11(1):2536.
- [52] Ho JC, Ghosh J, Sun J. Marble: High-throughput phenotyping from electronic health records via sparse nonnegative tensor factorization. In: *Proc. 20th ACM SIGKDD Int. Conf. Knowl. Discov. Data Min. KDD '14.* New York, NY, USA: ACM; 2014. p. 115–124.
- [53] Zhao J, Zhang Y, Schlueter DJ, Wu P, Eric Kerchberger V, Trent Rosenbloom S, et al. Detecting time-evolving phenotypic topics via tensor factorization on electronic health records: Cardiovascular disease case study. *Journal of Biomedical Informatics.* 2019 Oct;98:103270.
- [54] Haldar P, Pavord ID, Shaw DE, Berry MA, Thomas M, Brightling CE, et al. Cluster Analysis and Clinical Asthma Phenotypes. *Am J Respir Crit Care Med.* 2008 Aug;178(3):218–224.
- [55] Sutherland ER, Goleva E, King TS, Lehman E, Stevens AD, Jackson LP, et al. Cluster Analysis of Obesity and Asthma Phenotypes. *PLOS ONE.* 2012 May;7(5):e36631.
- [56] Ahmad T, Pencina MJ, Schulte PJ, O'Brien E, Whellan DJ, Piña IL, et al. Clinical implications of chronic heart failure phenotypes defined by cluster analysis. *J Am Coll Cardiol.* 2014 Oct;64(17):1765–1774.
- [57] Shah SJ, Katz DH, Selvaraj S, Burke MA, Yancy CW, Gheorghiane M, et al. Phenomapping for Novel Classification of Heart Failure With Preserved Ejection Fraction. *Circulation.* 2015 Jan;131(3):269–279.
- [58] Li L, Cheng WY, Glicksberg BS, Gottesman O, Tamler R, Chen R, et al. Identification of type 2 diabetes subgroups through topological analysis of patient similarity. *Sci Transl Med.* 2015 Oct;7(311):311ra174–311ra174.
- [59] Zinchuk A, Yaggi HK. Phenotypic Subtypes of OSA: A Challenge and Opportunity for Precision Medicine. *Chest.* 2020 Feb;157(2):403–420.
- [60] Hendricks R, Khasawneh M. Cluster Analysis of Categorical Variables of Parkinson's Disease Patients. *Brain Sci.* 2021 Oct;11(10):1290.
- [61] Landi I, Glicksberg BS, Lee HC, Cherng S, Landi G, Danieletto M, et al. Deep representation learning of electronic health records to unlock patient stratification at scale. *npj Digit Med.* 2020 Jul;3(1):1–11.

- [62] Jain AK. Data clustering: 50 years beyond K-means. *Pattern Recognit Lett.* 2010;31(8):651–666.
- [63] Agustí A. Phenotypes and Disease Characterization in Chronic Obstructive Pulmonary Disease. Toward the Extinction of Phenotypes? *Annals ATS.* 2013 Dec;10(Supplement):S125–S130.
- [64] Termsarasab P, Thammongkolchai T, Frucht SJ. Medical treatment of dystonia. *Journal of Clinical Movement Disorders.* 2016 Dec;3(1):19.
- [65] D’Amour A, Heller K, Moldovan D, Adlam B, Alipanahi B, Beutel A, et al. Underspecification Presents Challenges for Credibility in Modern Machine Learning. *J Mach Learn Res.* 2022;23(226):1–61. Available from: <http://jmlr.org/papers/v23/20-1335.html>.
- [66] Lasko TA, Strobl EV, Stead WW. Why Do Clinical Probabilistic Models Fail To Transport Between Sites?. *arXiv*; 2023.
- [67] Bergstra JS, Bardenet R, Bengio Y, Kégl B. Algorithms for hyper-parameter optimization. In: Shawe-Taylor J, Zemel RS, Bartlett PL, Pereira F, Weinberger KQ, editors. *Advances in neural information processing systems 24.* Curran Associates, Inc.; 2011. p. 2546–2554. Available from: <http://papers.nips.cc/paper/4443-algorithms-for-hyper-parameter-optimization.pdf>.
- [68] Bergstra J, Yamins D, Cox DD. Making a science of model search. *Proc 30th Int Conf Mach Learn ICML 13.* 2013 Sep;.
- [69] Himberg J, Hyvärinen A. Independent component analysis for binary data: An experimental study. In: *Proc. ICA2001*; 2001. p. 552–556.
- [70] Li TZ, Xu K, Chada NC, Chen H, Knight M, Antic S, et al. Curating Retrospective Multimodal and Longitudinal Data for Community Cohorts at Risk for Lung Cancer.. *medRxiv*; 2023.
- [71] Fritsch FN, Butland J. A Method for Constructing Local Monotone Piecewise Cubic Interpolants. *SIAM J Sci and Stat Comput.* 1984 Jun;5(2):300–304.
- [72] Bourel M, Fraiman R, Ghattas B. Random average shifted histograms. *Comput Stat Data Anal.* 2014;79(0):149–164.